Article

Energetics and Dynamics of Electron Transfer and Proton Transfer in Dissociation of Metal(salen)–Peptide Complexes in the Gas Phase

Julia Laskin, Zhibo Yang, and Ivan K. Chu

J. Am. Chem. Soc., **2008**, 130 (10), 3218-3230 • DOI: 10.1021/ja077690s

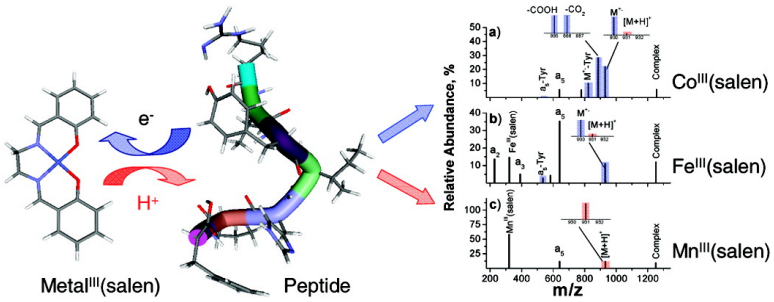

More About This Article

Additional resources and features associated with this article are available within the HTML version:

- Supporting Information
- Links to the 1 articles that cite this article, as of the time of this article download
- Access to high resolution figures
- Links to articles and content related to this article
- Copyright permission to reproduce figures and/or text from this article

View the Full Text HTML

J|A|C|S
ARTICLES
Published on Web 02/12/2008

Energetics and Dynamics of Electron Transfer and Proton Transfer in Dissociation of Metal^{III}(salen)−Peptide Complexes in the Gas Phase

Julia Laskin,*,† Zhibo Yang,† and Ivan K. Chu*,‡

Pacific Northwest National Laboratory, Fundamental Sciences Division, Richland, Washington, and Department of Chemistry, The University of Hong Kong, Hong Kong, China

Received October 5, 2007; E-mail: Julia.Laskin@pnl.gov; ivankchu@hku.hk

Abstract: Time- and collision energy-resolved surface-induced dissociation (SID) of ternary complexes of Co^{III}(salen)$^+$, Fe^{III}(salen)$^+$, and Mn^{III}(salen)$^+$ with several angiotensin peptide analogues was studied using a Fourier transform ion cyclotron resonance mass spectrometer (FT-ICR MS) specially equipped to perform SID experiments. Time-resolved fragmentation efficiency curves (TFECs) were modeled using an RRKM-based approach developed in our laboratory. The approach utilizes a very flexible analytical expression for the internal energy deposition function that is capable of reproducing both single-collision and multiple-collision activation in the gas phase and excitation by collisions with a surface. The energetics and dynamics of competing dissociation pathways obtained from the modeling provides important insight on the competition between proton transfer, electron transfer, loss of neutral peptide ligand, and other processes that determine gas-phase fragmentation of these model systems. Similar fragmentation behavior was obtained for various Co^{III}(salen)−peptide systems of different angiotensin analogues. In contrast, dissociation pathways and relative stabilities of the complexes changed dramatically when cobalt was replaced with trivalent iron or manganese. We demonstrate that the electron-transfer efficiency is correlated with redox properties of the metal^{III}(salen) complexes (Co > Fe > Mn), while differences in the types of fragments formed from the complexes reflect differences in the modes of binding between the metal−salen complex and the peptide ligand. RRKM modeling of time- and collision-energy-resolved SID data suggests that the competition between proton transfer and electron transfer during dissociation of Co^{III}(salen)−peptide complexes is mainly determined by differences in entropy effects while the energetics of these two pathways are very similar.

1. Introduction

Electron transfer and proton transfer are the most fundamental processes in chemistry and biology.[1] Electron transfer is particularly important in enzyme catalysis, photosynthesis, and respiration. Gas-phase decomposition of ternary complexes of transition metal ions with organic and peptide ligands provides a unique opportunity to explore the competition between these processes using relatively simple model systems. It can be also utilized for the formation of different types of odd-electron peptide ions for analytical applications focused on identification of peptides and proteins using mass spectrometry.[2]

Peptide and protein ions are traditionally introduced into the gas phase in the form of closed-shell protonated ions or ions cationized on metals using soft ionization techniques such as electrospray (ESI)[3] and matrix-assisted laser desorption ionization (MALDI).[4] Development of these ionization methods resulted in an explosive growth of studies that use mass spectrometry for identification and structural characterization of large molecules.[5−7] The most common strategy in these studies involves tandem mass spectrometry (MS/MS), which relies on structurally specific fragmentation of mass-selected ions in the gas phase. Collision-induced dissociation (CID) of peptide ions typically results in formation of *b*- and *y*-type backbone fragments.[8] In contrast, fragmentation of odd-electron $[M + nH]^{\bullet(n-1)+}$ ions produced by capture of low-energy electrons by $[M + nH]^{n+}$ results in formation of *c* and *z* ions.[9] Electron capture dissociation (ECD) is very attractive because it provides dissociation patterns that are complementary to CID and enables identification of post-translationally modified proteins.[10,11] It has been demonstrated that ECD is superior to CID for top-down characterization of proteins.[12,13]

† Pacific Northwest National Laboratory.
‡ The University of Hong Kong.

(1) Holm, R. H.; Kennepohl, P.; Solomon, E. I. *Chem. Rev.* **1996**, *96*, 2239−2314.
(2) Hopkinson, A. C.; Siu, K. W. M. Peptide Radical Cations. In *Principles of Mass Spectrometry Applied to Biomolecules*; Laskin, J., Lifshitz, C., Eds.; John Wiley & Sons: Hoboken, NJ, 2006.
(3) Fenn, J. B.; Mann, M.; Meng, C. K.; Wong, S. F.; Whitehouse, C. M. *Science* **1989**, *246*, 64−71.
(4) Hillenkamp, F.; Karas, M.; Beavis, R. C.; Chait, B. T. *Anal. Chem.* **1991**, *63*, A1193−A1202.
(5) Aebersold, R.; Goodlett, D. R. *Chem. Rev.* **2001**, *101*, 269−296.
(6) Hofstadler, S. A.; Griffey, R. H. *Chem. Rev.* **2001**, *101*, 377−390.
(7) McLuckey, S. A.; Wells, J. M. *Chem. Rev.* **2001**, *101*, 571−606.
(8) Wysocki, V. H.; Cheng, G.; Zhang, Q.; Herrmann, K. A.; Beardsley, R. L.; Hilderbrand, A. E. Peptide Fragmentation Overview. In *Principles of Mass Spectrometry Applied to Biomolecules*; Laskin, J., Lifshitz, C., Eds.; Wiley-Interscience: Hoboken, NJ, 2006.
(9) Kelleher, N. L.; Zubarev, R. A.; Bush, K.; Furie, B.; Furie, B. C.; McLafferty, F. W.; Walsh, C. T. *Anal. Chem.* **1999**, *71*, 4250−4253.
(10) McLafferty, F. W.; Horn, D. M.; Breuker, K.; Ge, Y.; Lewis, M. A.; Cerda, B.; Zubarev, R. A.; Carpenter, B. K. *J. Am. Soc. Mass Spectrom.* **2001**, *12*, 245−249.

 10.1021/ja077690s CCC: $40.75

Dissociation of peptide radical cations, $M^{\bullet+}$, is significantly different from the dissociation of the corresponding $[M + H]^+$ and $[M + 2H]^{\bullet+}$ ions.[14] However, until recently formation of peptide radical cations in the gas phase was tedious and could be performed only for selected species. Siu and co-workers demonstrated that redox chemistry of transition metal complexes can be utilized to generate $M^{\bullet+}$ peptide ions.[2,15,16] CID of ternary $Cu^{II}(L)$−peptide complexes (where L is a ligand) resulted in facile formation of radical cations of small model peptides and amino acids.[17−20] Properties of the ligand and the peptide composition play a major role in determining the fragmentation behavior of such complexes. For example, dissociation of $[Cu^{II}(dien)M]^{\bullet2+}$ complexes (dien = diethylenetriamine) results in facile electron transfer and abundant formation of the radical cation only for peptides containing tryptophan or tyrosine residues that have relatively low ionization energies; complexes with other peptides dissociate preferably through proton-transfer reactions. Proton-transfer reactions are especially important for peptides containing basic amino residues that can more readily abstract an acidic proton from the ligand. It has been demonstrated that proton transfer is strongly suppressed for ligands that do not possess protons attached to the coordinating nitrogen atoms such as *N*,*N*,*N*′,*N*′,*N*″-pentamethyldiethylenetriamine (Me_5dien) and 2,2′:6′,2″-terpyridine (terpy) and that the electron transfer and formation of peptide radical cations is facilitated by the presence of sterically encumbered auxiliary ligands such as 6,6″-dibromo-2,2′:6′,2″-terpyridine or 1,4,7,10-tetraoxacyclododecane (12-crown-4).[19−22]

Redox chemistry resulting in formation of odd-electron peptide ions is not limited to copper(II) complexes. For example, O'Hair and co-workers studied the formation of peptide radical cations containing basic amino residues from salen complexes of trivalent chromium, manganese, iron, and cobalt.[23] They reported that peptide radical cations could be formed from each metal complex. However, they found that dissociation of Mn and Fe complexes resulted in significantly higher yields of radical cation formation. Chu and co-workers demonstrated formation of negative $[M - 2H]^{-\bullet}$ ions from complexes of $Mn^{III}(salen)^+$ with doubly deprotonated peptide molecules.[24] Coordination of a trivalent metal with the salen ligand produces a singly charged complex **I**, which readily forms singly charged cationic complexes with neutral peptide molecules or anionic complexes with doubly deprotonated peptides that can be introduced into the gas phase using electrospray ionization.

Scheme 1

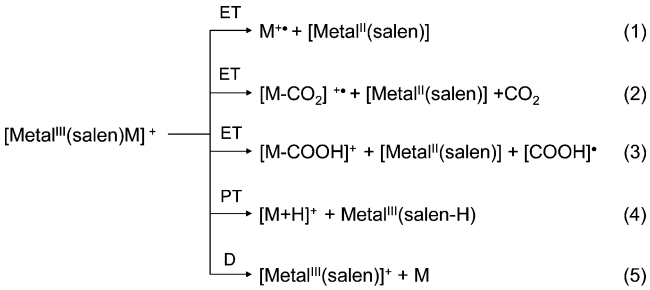

(a) Metal= **Co, Fe or Mn**

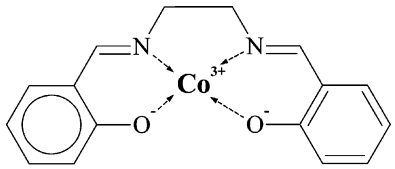

I

Several fragmentation pathways are commonly observed during collision-induced dissociation of the positively charged metal−salen complexes (Scheme 1).[23] These include proton transfer (PT) to the peptide molecule or to the ligand, reduction of the metal center followed by electron transfer (ET) from the peptide molecule and formation of the radical cation, dissociation of the complex into the $[metal^{III}(salen)]^+$ ion and neutral peptide molecule (D), and dissociative electron transfer resulting in formation of fragment ions of the corresponding peptide radical cation. Here we present a first detailed study of the energetics and dynamics of dissociation of positively charged $metal^{III}$(salen)−peptide complexes in the gas phase using time- and collision-energy-resolved surface induced dissociation (SID) experiments combined with RRKM modeling. We examine factors that affect the competition between proton-transfer and electron-transfer processes in gas-phase fragmentation of these model systems.

2. Experimental Section

2.1. Ion Trap Experiments. Ion trap experiments were conducted using a quadrupole ion trap mass spectrometer (Finnigan LCQ, ThermoFinnigan, San Jose, CA). Samples were continuously infused at a rate of 5 μL/min into the pneumatically assisted electrospray probe using air as the nebulizer gas. CID spectra were acquired using helium as the collision gas. The injection and activation times for CID in the ion trap were 200 and 30 ms, respectively; the amplitude of the excitation was optimized for each experiment.

2.2. FT-ICR Experiments. SID experiments were conducted on a specially fabricated 6T FT-ICR mass spectrometer described in detail elsewhere.[25] The instrument is equipped with a high-transmission electrospray source, consisting of an ion funnel interface[26] followed by three quadrupoles that provide for pressure drop and ion bunching, mass selection, and ion storage, respectively. The SID target is introduced through a vacuum interlock assembly and is positioned at

(11) Zubarev, R. Electron Capture Dissociation and Other Ion-Electron Fragmentation Reactions. In *Principles of Mass Spectrometry Applied to Biomolecules*; Laskin, J., Lifshitz, C., Eds.; Wiley-Interscience: Hoboken, NJ, 2006.
(12) Ge, Y.; Lawhorn, B. G.; ElNaggar, M.; Strauss, E.; Park, J. H.; Begley, T. P.; McLafferty, F. W. *J. Am. Chem. Soc.* **2002**, *124*, 672−678.
(13) Zubarev, R. A. *Mass Spectrom. Rev.* **2003**, *22*, 57−77.
(14) Laskin, J.; Yang, Z.; Lam, C.; Chu, I. K. *Anal. Chem.* **2007**, *79*, 6607−6614.
(15) Chu, I. K.; Rodriquez, C. F.; Lau, T. C.; Hopkinson, A. C.; Siu, K. W. M. *J. Phys. Chem. B* **2000**, 104, 3393−3397.
(16) Bagheri-Majdi, E.; Ke, Y. Y.; Orlova, G.; Chu, I. K.; Hopkinson, A. C.; Siu, K. W. M. *J. Phys. Chem. B* **2004**, *108*, 11170−11181.
(17) Hopkinson, A. C.; Siu, K. W. M. Peptide Radical Cations. In *Principles of Mass Spectrometry Applied to Biomolecules*; Laskin, J., Lifshitz, C., Eds.; Wiley-Interscience: Hoboken, NJ, 2006.
(18) Barlow, C. K.; Wee, S.; McFadyen, W. D.; O'Hair, R. A. J. *Dalton Trans.* **2004**, 3199−3204.
(19) Chu, I. K.; Lam, C. N. W.; Siu, S. O. *J. Am. Soc. Mass Spectrom.* **2005**, *16*, 763−771.
(20) Barlow, C. K.; Moran, D.; Radom, L.; McFadyen, W. D.; O'Hair, R. A. J. *J. Phys. Chem. A* **2006**, *110*, 8304−8315.
(21) Chu, I. K.; Lam, C. N. W. *J. Am. Soc. Mass Spectrom.* **2005**, *16*, 1795−1804.
(22) Chu, I. K.; Siu, S. O.; Lam, C. N. W.; Chan, J. C. Y.; Rodriquez, C. F. *Rapid Commun. Mass Spectrom.* **2004**, *18*, 1798−1802.
(23) Barlow, C. K.; McFadyen, W. D.; O'Hair, R. A. J. *J. Am. Chem. Soc.* **2005**, *127*, 6109−6115.
(24) Lam, C. N. W.; Chu, I. K. *J. Am. Soc. Mass Spectrom.* **2006**, *17*, 1249−1257.
(25) Laskin, J.; Denisov, E. V.; Shukla, A. K.; Barlow, S. E.; Futrell, J. H. *Anal. Chem.* **2002**, *74*, 3255−3261.
(26) Shaffer, S. A.; Tang, K. Q.; Anderson, G. A.; Prior, D. C.; Udseth, H. R.; Smith, R. D. *Rapid Commun. Mass Spectrom.* **1997**, *11*, 1813−1817.

the rear trapping plate of the ICR cell. Samples are electrosprayed, at atmospheric pressure, into the end of a heated stainless steel capillary tube. The ion funnel that follows the capillary provides highly efficient transfer of ions exiting the capillary into the high vacuum region of the mass spectrometer. Three quadrupoles following the ion funnel provide collisional focusing, mass selection of the ion of interest, and accumulation of ions external to the ICR cell. Typical accumulation times are in the range 1−3 s. The third (accumulation) quadrupole is held at elevated pressure (about 2×10^{-3} Torr) for collisional relaxation of any internal energy possessed by ions generated by electrospray ionization prior to their injection into the ICR cell.

After accumulation, the ions are extracted from the third quadrupole and transferred into the ICR cell where they collide with the surface. Scattered ions are captured by raising the potentials on the front and rear trapping plates of the ICR cell by 10−20 V. Time-resolved mass spectra are acquired by varying the delay between the gated trapping and the excitation/detection event (the reaction delay). The reaction delay is varied from 1 ms to 1 s. Immediately following the fragmentation delay, ions are excited by a broadband chirp and detected. The collision energy is defined by the difference in the potential applied to the accumulation quadrupole and the potential applied to the rear trapping plate and the SID target. The ICR cell can be offset above or below ground by as much as ±150 V. Lowering the ICR cell below ground while keeping the potential on the third quadrupole fixed increases collision energy for positive ions.

Experimental control is accomplished with a MIDAS data station developed by Marshall and co-workers at the National High Magnetic Field Laboratory.[27] MIDAS is used to control the voltages and timing of the source and transfer optics, as well as ion manipulation in the ICR cell. An automated script was written to allow for unattended acquisition of kinetic data. The script was used to vary the fragmentation delay and collision energy of the experiment. Reactions delays of 1 ms, 5 ms, 10 ms, 50 ms, 0.1 s, and 1 s were studied. Typical experiments involved changing the collision energy from 21 to 68 eV in 1.5 eV increments at each of the six fragmentation delays. Time dependent survival curves were constructed from experimental mass spectra by plotting the relative abundance of the precursor ion as a function of collision energy for each delay time.

2.3. SID Target. The self-assembled monolayer surface of 1-dodecanethiol (HSAM) was prepared on a single gold {111} crystal (Monocrystals, Richmond Heights, OH) using a standard procedure. The target was cleaned in a UV cleaner (model 135500, Boekel Industries Inc., Feasterville, PA) for 10 min and allowed to stand in a solution of 1-dodecanethiol for 10 h. The target was removed from the SAM solution and washed ultrasonically in ethanol for 10 min to remove extra layers.

2.4. Chemicals. All chemicals and reagents were commercially available (Sigma-Aldrich, St. Louis, MO; Bachem, King of Prussia, PA). Angiotensin II (DRVYIHPF) and angiotensin III (RVYIHPF) were purchased from Sigma/Aldrich (St. Louis, MO). RVYIHDF was purchased from Peptron Inc. (Taejon, South Korea). Fmoc-Protected amino acids and the Wang resin were purchased from Advanced ChemTech (Louisville, KY). Several angiotensin derivatives were synthesized according to literature procedures.[28] Synthesis of *N*,*N*′-ethylenebis(salicylideneaminato) and metal(III)−salen complexes [salen = *N*,*N*′-ethylenebis(salicylideneaminato)] followed the procedure described elsewhere.[29] Samples typically comprised 600 μM metal(III)−salen complex and 50 μM peptide in a water/methanol (50:50) solution. A syringe pump (Cole Parmer, Vernon Hills, IL) was used for direct infusion of the electrospray samples at flow rates ranging from 30 to 50 μL/h.

2.5. Theoretical Calculations. Preliminary structures of the neutral Arg-Val-Tyr tripeptide terminated with the methyl group (RVY-Me) were obtained using molecular dynamics stimulated annealing within the Insight II package (Biosym Technologies, San Diego, CA). Subsequent density functional theory (DFT) calculations were carried out using NWChem (version 5.0) developed and distributed by the Pacific Northwest National Laboratory (PNNL).[30] DFT calculations were used for geometry optimization, single-point energy, and frequency calculations for the model tripetide and the metal−salen complex. Geometry optimizations and frequency calculations for the neutral peptide and the corresponding radical cation were carried out at the B3LYP/6-31G(d) level of theory, while single-point energy calculations were performed at the B3LYP/6-31++G(d,p) level of theory. B3LYP/6-31++G(d,p)) was used to describe O, N, C, and H atoms of Co^{II}-(salen) and Co^{III}(salen) complexes, while effective core potential (ECP) with the Stuttgart RSC 1997 basis set[31] was employed for the Co atom. Zero-point energy (ZPE) corrections to the energies were derived from the calculated vibrational frequencies. All the optimized structures were visualized using the Extensible Computational Chemistry Environment (ECCE) developed at PNNL.[32]

2.6. RRKM Modeling. Time dependent survival curves (SCs) for the precursor ion and fragmentation efficiency curves (TFECs) for individual fragments were constructed from experimental mass spectra by plotting the relative abundance of the corresponding ion as a function of collision energy for each delay time. SCs and TFECs were modeled using an RRKM-based approach as described previously:[33,34]

(1) The microcanonical rate coefficient $k(E)$ is calculated as a function of internal energy using the RRKM/QET expression:

$$k(E) = \frac{\sigma W^{\ddagger}(E - E_0)}{h\rho(E)} \tag{1}$$

where $\rho(E)$ is the density of states of the reactant, $W^{\ddagger}(E - E_0)$ is the sum of states of the transition state, E_0 is the critical energy, h is Planck's constant, and σ is the reaction path degeneracy.

(2) The survival probability of the precursor ion and the probability for the formation of fragment ions as a function of the internal energy of the precursor ion and the experimental observation time (t_r), $F_i(E, t_r)$, were calculated from the rate-energy $k(E)$ dependency taking into account radiative decay of the excited ion population. The function $F_i(E, t_r)$ is commonly referred to as a breakdown curve. A collection of breakdown curves, called the breakdown graph (BDG), was then constructed from the individual breakdown curves calculated for each reaction channel.

(3) The internal energy deposition function was described by the following analytical expression:

$$P(E,E_{\text{coll}}) = \frac{1}{C}(E - \Delta)^l \exp\left(-\frac{(E - \Delta)}{f(E_{\text{coll}})}\right) \tag{2}$$

where l and Δ are parameters, $C = \Gamma(l + 1)[f(E_{\text{coll}})]^{l+1}$ is a normalization factor, and $f(E_{\text{coll}})$ has the form

$$f(E_{\text{coll}}) = A_2 E_{\text{coll}}{}^2 + A_1 E_{\text{coll}} + A_0 \tag{3}$$

where A_0, A_1, and A_2 are parameters, and E_{coll} is the collision energy.

(27) Senko, M. W.; Canterbury, J. D.; Guan, S. H.; Marshall, A. G. *Rapid Commun. Mass Spectrom.* **1996**, *10*, 1839−1844.
(28) Chan, W. C.; White, P. D. In *Fmoc Solid Phase Peptide Synthesis: A Practical Approach*; Oxford University Press: Oxford, New York, 2000.
(29) Varkey, S. P.; Ratnasamy, C.; Ratnasamy, P. *J. Mol. Catal. A: Chem.* **1998**, *135*, 295−306.
(30) Bylaska, E. J. et al. *NWChem, A Computational Chemistry Package for Parallel Computers*, version 5.0; Pacific Northwest National Laboratory: Richland, WA 99352-0999, U.S.A., 2006.
(31) Dolg, M.; Wedig, U.; Stoll, H.; Preuss, H. *J. Chem. Phys.* **1987**, *86*, 866.
(32) Black, G. et al. *Ecce, A Problem Solving Environment for Computational Chemistry, Software*, version 4.0.1; Pacific Northwest National Laboratory: Richland, WA 99352−0999, U.S.A., 2006.
(33) Laskin, J.; Byrd, M.; Futrell, J. H. *Int. J. Mass Spectrom.* **2000**, *196*, 285−302.
(34) Laskin, J.; Futrell, J. H. *J. Phys. Chem. A* **2000**, *104*, 5484−5494.

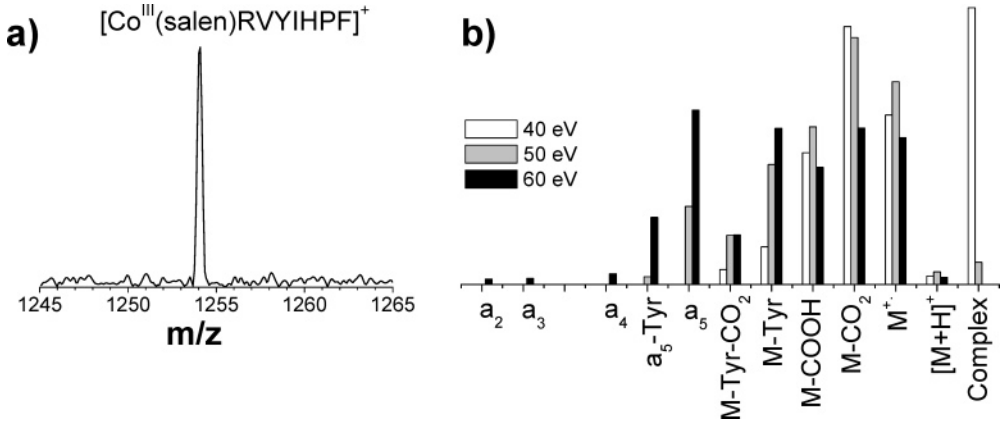

Figure 1. (a) Mass selected Co^{III}(salen)RVYIHPF precursor ion and (b) fragment distribution for SID of Co^{III}(salen)RVYIHPF complex on the HSAM surface at three collision energies.

We have shown previously that this analytical form for the collisional energy deposition function has enough flexibility to reproduce experimental fragmentation efficiency curves obtained using both gas-phase collisional activation and SID.[33,35,36] An exponential function obtained with $l = 0$ can be used to model single-collision CID experiments, while a Boltzmann-like function (high values of l) has been utilized to reproduce multiple-collision CID and SID data.

Collisional activation produces ions with a wide distribution of internal energies, P(E,E$_{Coll}$). The contribution of ions having internal energy E to the observed signal intensity for a particular reaction channel i equals $F_i(E, t_r)$ $P(E, E_{Coll})$. Integrating over internal energies yields an overall signal intensity at a given center-of-mass (CM) collision energy, $I(E_{Coll})$:

$$I_i(E_{coll}) = \int_0^\infty F_i(E,t)\, P(E,E_{coll})\, \mathrm{d}E \qquad (4)$$

Vibrational frequencies of the precursor ions were estimated by combining the frequencies of an unbound peptide with the frequencies of the metal−salen complex. Vibrational frequencies of the unbound peptide were adopted from our previous study.[37] Frequencies of the cobalt−salen complex were obtained from the DFT calculations described earlier. The same frequency ensemble was utilized for the iron−salen and manganese−salen complexes. Vibrational frequencies for the transition state were estimated by removing one C−N stretch (reaction coordinate) from the parent ion frequencies as well as varying all frequencies in the range of 500−1000 cm^{-1} to obtain the best fit with experimental data.

SCs were constructed using the above procedure and compared to the experimental data. The internal energy deposition function was determined by fitting the experimental SCs of the singly protonated RVYIHPF, for which the dissociation parameters are known from our previous study[37] and kept the same for all reaction times. The fitting parameters included the critical energy and activation entropy for dissociation of the precursor ion (eqs 2,3). They were varied until the best fit to experimental SCs was obtained. The uniqueness of the fits was confirmed using the sensitivity analysis described elsewhere.[34]

3. Results

In this study we examined CID and SID of singly charged metal^{III}(salen) complexes of trivalent cobalt, iron, and manganese with neutral peptides: angiotensin II (DRVYIHPF), angiotensin III (RVYIHPF), and several analogues. Most of the SID and CID experiments reported here were performed using isotopically selected precursor ions. This is an important prerequisite for quantitative comparison between the efficiency of proton transfer and electron transfer during dissociation of the complexes because the product ions formed in these reactions, M$^{+\bullet}$ and [M + H]$^+$, are separated only by one mass unit and the [M + H]$^+$ peak overlaps with the ^{13}C isotope of the M$^{+\bullet}$ ion. However, in some experiments the isotopically resolved signal was too low for time-resolved SID studies. In this case, the relative abundance of the [M + H]$^+$ peak observed experimentally was corrected by subtracting the contribution of the second isotope of the M$^{+\bullet}$ peak.

3.1. Dissociation Pathways. 3.1.1. Co^{III}(salen) Complexes. A mass-selected [Co^{III}(salen)RVYIHPF]$^+$ precursor ion and its SID fragment distributions obtained at three collision energies are shown in Figure 1. The four primary dissociation pathways of the complex resulting in formation of M$^{+\bullet}$, M$^{+\bullet}$−CO$_2$, [M−COOH]$^+$, and [M + H]$^+$ fragment ions at low collision energies are summarized in Scheme 1 (reactions 1−4). Losses of CO$_2$ and COOH$^\bullet$ are characteristic dissociation pathways of peptide radical cations[17,23,38] that have been previously observed for dissociation of both doubly charged and singly charged ternary complexes of transition metals with peptides.[15,23,39,40] Formation of these ions requires electron transfer (ET) from the peptide to the metal core of the complex. In addition, ET results in formation of the peptide radical cation, M$^{+\bullet}$, while the [M + H]$^+$ ion is formed by proton transfer (PT) from the organic ligand to the peptide.

Figure 2 shows collision energy-resolved SID data for [Co^{III}(salen)RVYIHPF]$^+$ obtained at a reaction delay of 1 s. M$^{+\bullet}$−CO$_2$ is the most abundant primary fragment ion produced from the complex. Similar yields are observed for the formation of M$^{+\bullet}$ and [M−COOH]$^+$ ions over a broad range of collision energies, while the [M + H]$^+$ fragment corresponding to the proton-transfer channel has the highest appearance energy among the four primary channels and is not as abundant as primary fragments produced following electron transfer. It follows that electron transfer is the dominant process during dissociation of the [Co^{III}(salen)RVYIHPF]$^+$ complex.

(35) Laskin, J.; Denisov, E.; Futrell, J. *J. Am. Chem. Soc.* **2000**, *122*, 9703−9714.
(36) Laskin, J.; Denisov, E.; Futrell, J. H. *Int. J. Mass Spectrom.* **2002**, *219*, 189−201.
(37) Laskin, J.; Bailey, T. H.; Futrell, J. H. *Int. J. Mass Spectrom,*. **2004**, *234*, 89−99.
(38) Wee, S.; O'Hair, R. A. J.; McFadyen, W. D. *Int. J. Mass Spectrom.* **2004**, *234*, 101−122.
(39) Gatlin, C. L.; Turecek, F.; Vaisar, T. *J. Mass Spectrom.* **1995**, *30*, 1605−1616.
(40) Hu, P. F.; Loo, J. A. *J. Am. Chem. Soc.* **1995**, *117*, 11314−11319.

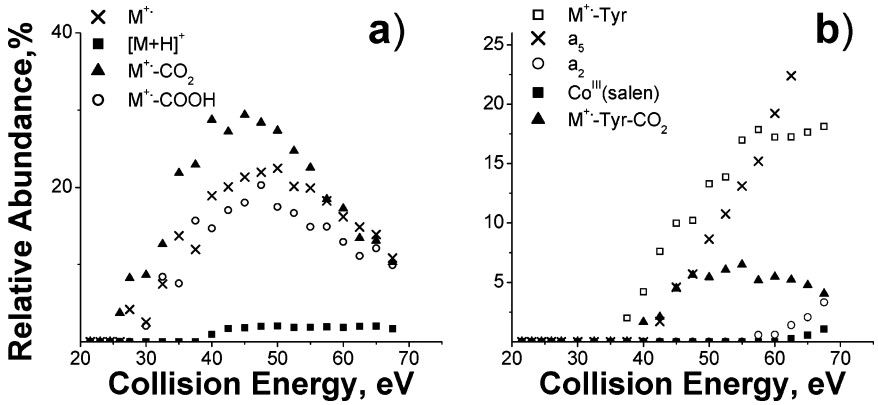

Figure 2. Collision energy-resolved SID data for (a) primary and (b) secondary fragment ions of Co^{III}(salen)RVYIHPF at 1 s reaction delay.

Several other fragments are observed at higher collision energies (Figures 1b and 2b). These include the loss of *p*-quinomethide (Tyr) from the tyrosine side chain of the radical cation and the $M^{+\bullet}-CO_2$ ion resulting in formation of the $M^{+\bullet}-$Tyr and $M^{+\bullet}-CO_2-$Tyr product ions, respectively, the formation of $\mathbf{a_2}$, $\mathbf{a_3}$, $\mathbf{a_4}$, and $\mathbf{a_5}$ backbone fragments and the $Co^{III}(salen)^+$ product ion (reaction 5, Scheme 1). MS^3 experiments (data not shown) suggest that **a**-ions can be formed from both $M^{+\bullet}$ and $M^{+\bullet}-CO_2$ primary fragments. Dissociation of the complex into its constituents, $Co^{III}(salen)^+$ and neutral RVYIHPF, is a very minor channel observed at high collision energies. It should be noted that the $M^{+\bullet}-$Tyr fragment ion could be produced both directly from the $[Co^{III}(salen)RVYIHPF]^+$ complex and by consecutive fragmentation of the $M^{+\bullet}$ ion. However, because the appearance energy of this fragment is ca. 8 eV higher than the appearance energy for the formation of the $M^{+\bullet}$ ion, it is reasonable to assume that this ion is mainly produced as a secondary dissociation product of the radical cation.

Formation of abundant $M^{+\bullet}-CO_2$ and $[M-COOH]^+$ fragments from the $[Co^{III}(salen)RVYIHPF]^+$ complex most likely involves ET from the C-terminal carboxylic group followed by fast fragmentation of the unstable carboxyl radical.[17,38] We further explored the role of the COOH group on the fragmentation behavior of $Co^{III}(salen)-$peptide complexes by examining the SID of several complexes that contain two carboxylic groups: the C-terminal carboxyl group and the COOH group of the aspartic acid side chain. Fragment distributions resulting from 40 eV collisions of $Co^{III}(salen)$ complexes with RVYIHPF, DRVYIHPF, and RVYIHDF with the HSAM surface are shown in Figure 3. The striking similarity between the fragment distributions obtained for the peptide containing one carboxyl group (RVYIHPF) and peptides containing two carboxyl groups (DRVYIHPF and RVYIHDF) suggests that the COOH group of the acidic side chain is not involved in the $Co^{III}(salen)-$peptide binding.

Dissociation of cobalt−salen−peptide complexes studied in this work is dominated by reactions 1−3 that involve the reduction of the metal−salen complex, while reactions 4 and 5 are minor channels in gas-phase fragmentation of these complexes. Average branching ratios of the products of reactions 4 and 5 for three different peptides are shown in Table 1. The formation of the $Co^{III}(salen)^+$ product via reaction 5 is observed at high collision energies, and the relative abundance of this fragment is 22−35 times lower than the abundance of the $M^{+\bullet}$ ion. The PT pathway (reaction 4) shows a larger variation with the structure of the peptide ligand. Specifically, the largest yield of the $[M + H]^+$ fragment (ca. 20% of the $M^{+\bullet}$ ion) is obtained for RVYIHDF, and the lowest yield (<5%) is obtained for DRVYIHPF.

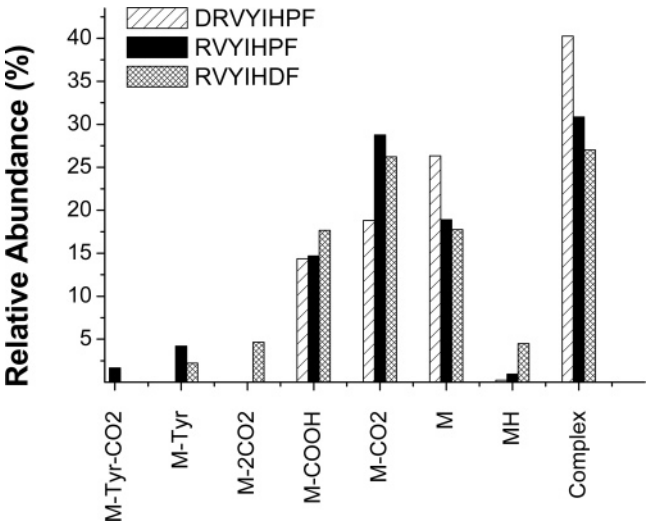

Figure 3. Comparison of 40 eV, 1 s SID fragment distributions obtained for complexes of Co^{III}(salen) with RVYIHPF, RVYIHDF, and DRVYIHPF.

Table 1. Average Branching Ratios between the Products of Reaction 1 and Reactions 4 and 5 (Scheme 1) for Three Peptides Studied in This Work Obtained for Reaction Delay of 1 s

peptide	$M^{+\bullet}/[M+H]^+$	$M^{+\bullet}/Co^{III}(salen)^+$
RVYIHPF	10	30
DRVYIHPF	20	35
RVYIHDF	5	22

3.1.2. Role of Tyrosine. The role of individual amino acid residues on the dissociation behavior of $Co^{III}(salen)-$peptide complexes was explored using systematic substitution of several residues that are potentially involved in the metal binding. These experiments demonstrated that replacement of proline with alanine, histidine with phenylalanine, and arginine with histidine does not have a significant effect on the gas-phase fragmentation of the complexes suggesting that proline, histidine, and arginine do not participate in peptide binding to the $[Co^{III}(salen)]^+$. In contrast, the tyrosine residue has a major effect on the relative yield of the ET pathway (reaction 1) resulting in formation of

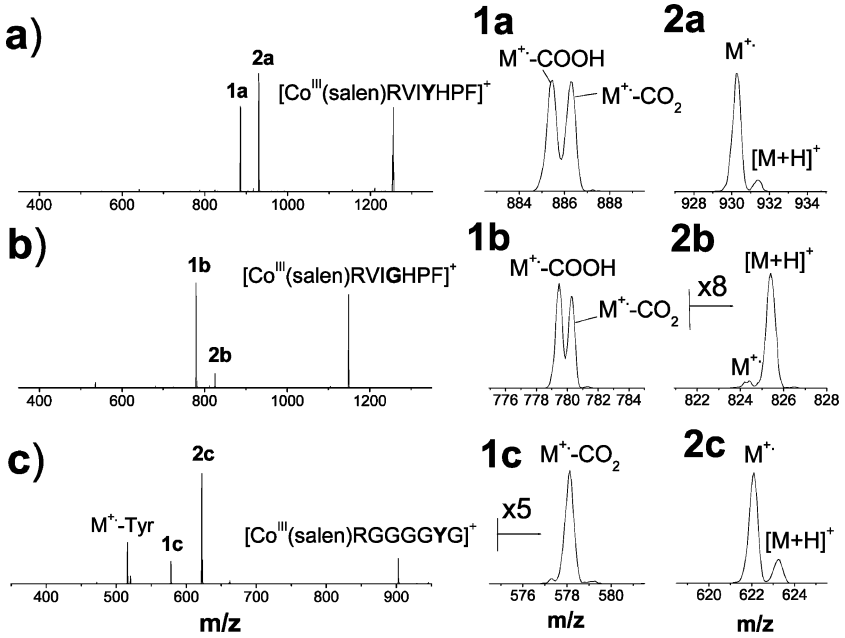

Figure 4. Ion trap MS/MS spectra of the (a) [Co^{III}(salen)RVIYHPF]$^+$, (b) [Co^{III}(salen)RVIGHPF]$^+$, and (c) [Co^{III}(salen)RGGGGYG]$^+$complexes.

the M$^{+\bullet}$ radical cation. This is illustrated in Figure 4 that compares ion trap MS/MS spectra of the cobalt−salen complexes of RVIYHPF and its analogue, RVIGHPF, in which tyrosine has been replaced with glycine. The spectra are dominated by the peaks corresponding to the four primary dissociation pathways (reactions 1−4). Substitution of the tyrosine with glycine results in significant suppression of the product of reaction 1; the relative abundance of the M$^{+\bullet}$ ion is reduced by a factor of 200. However, the formation of the M$^{+\bullet}$−CO_2 and [M−COOH]$^+$ fragment ions is not affected by the presence of the tyrosine residue in the sequence. Figure 4c shows an MS/MS spectrum of the [Co^{III}(salen)RGGGGYG]$^+$ complex. The spectrum obtained for this complex differs from the spectra obtained for other tyrosine-containing peptides studied in this work by substantial suppression of the M$^{+\bullet}$−CO_2 and the absence of the [M−COOH]$^+$ fragment ion, the major product ions observed for all other complexes. It should be also noted that very similar yields of the proton-transfer channel (about 15% of the precursor ion) resulting in formation of the [M + H]$^+$ ion are observed for all three complexes under similar experimental conditions. A similar result was obtained for dissociation of the [Co^{III}(salen)RGGGGGG]$^+$ complex (not shown). However, as expected from the earlier discussion the M$^{+\bullet}$ ion is also strongly suppressed in the MS/MS spectrum of this complex. Our results are consistent with previous study by Barlow et al.[23] that showed similar suppression of the M$^{+\bullet}$ ion in dissociation of [Co^{III}(salen-OMe)XGGFLR]$^+$ complexes for X = Tyr, Trp, and Gly. Abundant formation of the M$^{+\bullet}$ ion was observed only for the YGGFLR peptide ligand, while proton transfer and formation of M$^{+\bullet}$−CO_2 and [M−COOH]$^+$ fragments were dominant fragmentation channels for WGGFLR and GGGFLR.

3.1.3. Fe^{III}(salen) and Mn^{III}(salen) Complexes. Redox properties of the metal complexes and the mode of peptide binding in the ternary complex may have a pronounced effect on the branching ratios between different dissociation pathways shown in Scheme 1. O'Hair and co-workers demonstrated that dissociation of trivalent manganese− and iron−salen complexes

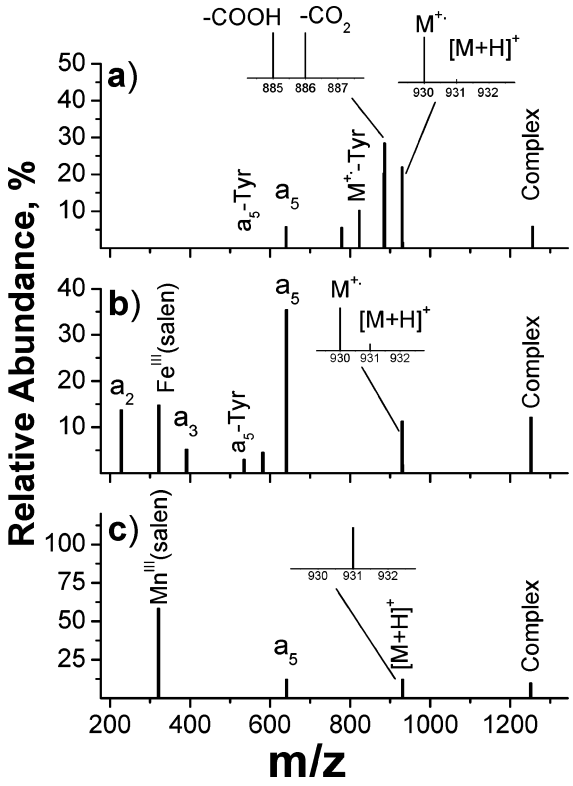

Figure 5. Fragment distributions corresponding to 90% fragmentation of (a) Co^{III}(salen) RVYIHPF (E_{coll} = 48.5 eV), (b) Fe^{III}(salen)RVYIHPF (E_{coll} = 90.5 eV), and (c) Mn^{III}(salen)RVYIHPF (E_{coll} = 80.5 eV).

with YGGFLR results in more efficient formation of radical cations as compared to dissociation of the [Co^{III}(salen)-YGGFLR]$^+$ complex.[23] In this study we examined the effect of the metal−salen complex on the stability and dissociation pathways of ternary complexes using RVYIHPF as a model system. SID patterns corresponding to 90% fragmentation of the precursor ion for complexes of RVYIHPF with [Co^{III}-(salen)]$^+$, [Fe^{III}(salen)]$^+$, and [Mn^{III}(salen)]$^+$ are shown in Figure 5. Spectra corresponding to a high extent of fragmentation were

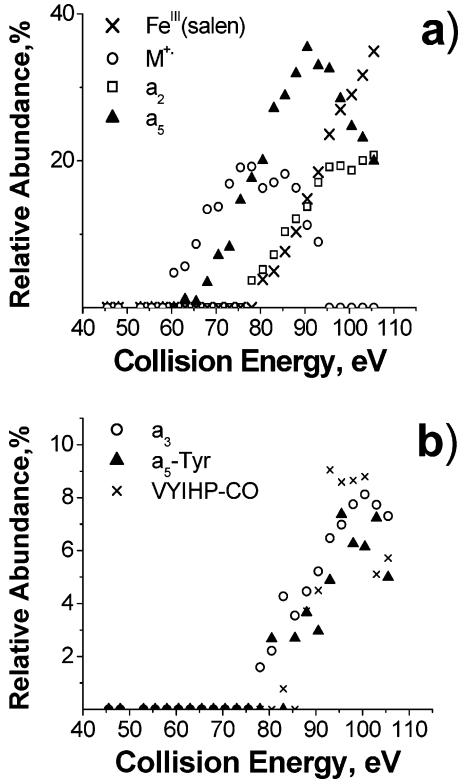

Figure 6. Collision energy-resolved SID data for (a) primary and (b) secondary fragment ions of Fe^{III}(salen)RVYIHPF at 1 s reaction delay.

selected because they contain all fragment ions observed in our time- and collision-energy-resolved experiments. Clearly, very different fragment distributions are obtained for the three complexes.

At low collision energies fragmentation of the [Fe^{III}(salen)-RVYIHPF]$^+$ complex results in formation of the radical cation along with the $\mathbf{a_5}$ ion (Figure 6a). Higher-energy fragments include $\mathbf{a_2}$, $\mathbf{a_3}$, $\mathbf{a_5}$-Tyr, internal a-ion (VYIHP−CO), and abundant Fe^{III}(salen)$^+$ fragment (Figure 6b). The peak corresponding to the PT channel was observed in SID spectra, but it was too weak to obtain reliable collision energy-resolved data. Interestingly, the products of dissociative electron-transfer channels (reactions 2 and 3) resulting in the formation of M$^{+\bullet}$−CO$_2$ and [M−COOH]$^+$ fragments—dominant reaction pathways for the cobalt-salen complex—were not observed for the iron−salen complex. These fragment ions are also absent in the SID spectrum of the [Mn^{III}(salen)RVYIHPF]$^+$ complex shown in Figure 5c. Dissociation of the this complex is dominated by the formation of the Mn^{III}(salen)$^+$ fragment (reaction 5) over a broad range of collision energies (Figure 7). Minor fragments of the Mn^{III}(salen)RVYIHPF complex include [M + H]$^+$ and $\mathbf{a_5}$ ions. PT is observed only at collision energies above 70 eV, while the ET pathways (reactions 1−3) are completely suppressed. Preferential formation of the Mn^{III}-(salen)$^+$ fragment ion has been also reported by Barlow et al.[23]

3.2. Relative Stability of Metal^{III}(salen)-Peptide Complexes. Kinetic experiments were conducted by varying the time delay between the ion-surface collision and the detection event in the range from 1 ms to 1 s. Time-resolved survival curves (SCs) were obtained by plotting the relative abundance of the intact precursor ion as a function of collision energy at different reaction delays. The relative position of the SCs reflects the

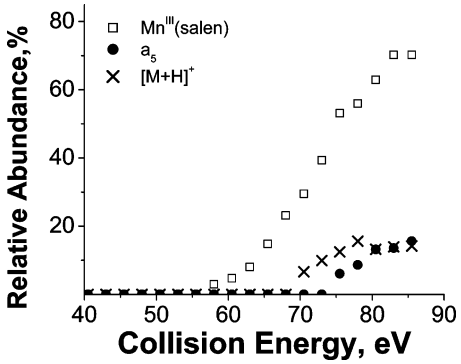

Figure 7. Collision energy-resolved SID data for fragment ions of Mn^{III}-(salen)RVYIHPF at 1 s reaction delay.

relative stability of different complexes toward fragmentation. The SCs obtained for cobalt−salen complexes with three different peptides at reaction delays of 1 ms and 1 s are shown in Figure 8a and 8b, respectively. The experimental SCs for [Co^{III}(salen)DRVYIHPF]$^+$ are slightly shifted toward higher collision energies for both 1 ms and 1 s reaction delays, while SCs obtained for cobalt−salen complexes of RVYIHPF and RVYIHDF show an almost perfect overlap. It should be noted that this trend follows the trend in the number of vibrational degrees of freedom (DOF) of the complexes (540 for DRVYIHPF, 501 for RVYIHPF, and 498 for RVYIHDF). The DOF effect can be eliminated by plotting the relative abundance of the precursor ion as a function of collision energy scaled by the number of DOF of the precursor ion. Perfect overlap between the SCs plotted vs the scaled collision energy (Figure 8c, d) clearly demonstrates that the observed shift in the position of the SCs shown in Figure 8a and 8b results only from the DOF effect and suggests that both the energetics and dynamics of dissociation of all three cobalt−salen−peptide complexes are very similar.

In contrast, the properties of the metal complex have a significant effect on the relative stability of the Metal(III)−salen−peptide complexes. The SCs of the [Mn^{III}(salen)RVYI-HPF]$^+$ shown in Figure 9 are shifted by more than 30 eV, and the SCs of the [Fe^{III}(salen)RVYIHPF]$^+$ complex are shifted by more than 40 eV toward higher collision energies as compared to the SCs of the [Co^{III}(salen)RVYIHPF]$^+$ complex. It is interesting to note that in addition to the differences in the energetics of fragmentation of Metal(III)−salen−peptide complexes, the kinetics of formation of common fragment ions from different complexes is quite different. For example, very fast kinetics of the formation of the M$^{+\bullet}$ ion was observed for the [Co^{III}(salen)RVYIHPF]$^+$ complex (Figure 10a), while the formation of the radical cation from the [Fe^{III}(salen)RVYIHPF]$^+$ complex follows a kinetically hindered pathway (Figure 10b) suggesting that this reaction requires substantial rearrangement of the complex.

3.3. RRKM Modeling Results. Quantitative description of the energetics and dynamics of decomposition of Metal(III)−salen−peptide complexes was obtained by modeling the experimental survival curves (SCs) using the RRKM based method outlined earlier. Relative stability of the complexes toward dissociation was obtained from the modeling of SCs of different precursor ions, while more detailed modeling of the time-resolved fragmentation efficiency curves (TFECs) of individual

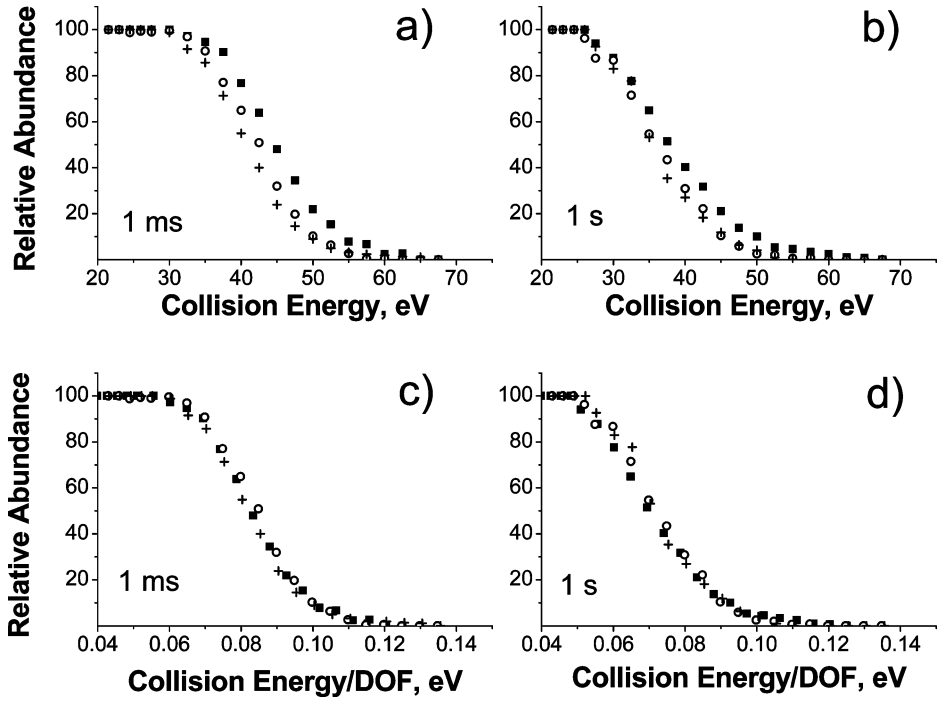

Figure 8. Survival curves (SCs) (panels a and b) and SCs plotted as a function of collision energy scaled by the number of the vibrational degrees of freedom of the precursor ion (panels c and d) for Co^{III}(salen)DRVYIHPF (■), Co^{III}(salen)RVYIHPF (○), and Co^{III}(salen)RVYIHDF (+), 1 ms (left panels) and 1 s (right panels).

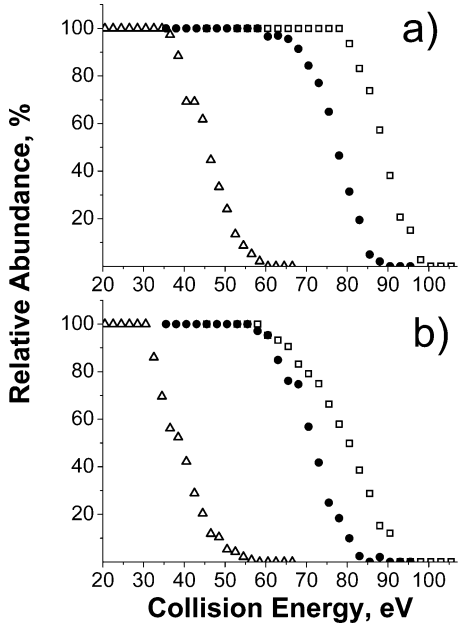

Figure 9. Experimental SID survival curves (SCs) for singly charged complexes of Co^{III}(salen) (△), Mn^{III}(salen) (●), and Fe^{III}(salen) (□) with RVYIHPF following collisions with the HSAM surface for reaction delay times of (a) 1 ms and (b) 1 s.

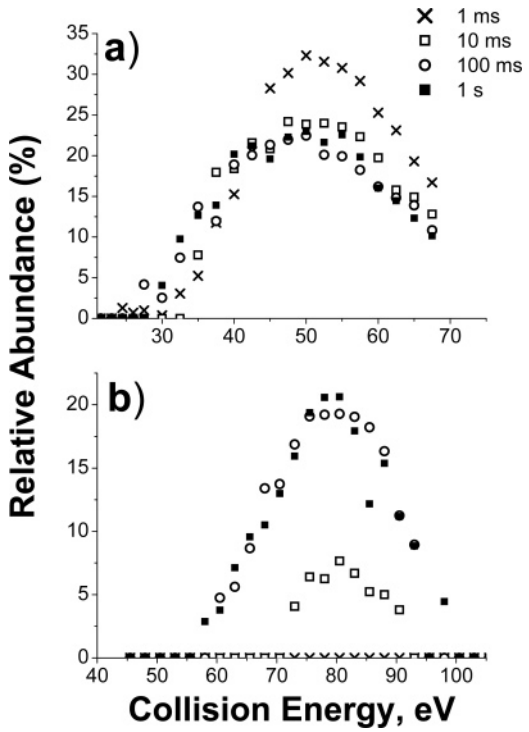

Figure 10. Experimental TFECs for the formation of the M$^{+\bullet}$ ion from the (a) [Co^{III}(salen)RVYIHPF]$^+$ and (b) [Fe^{III}(salen)RVYIHPF]$^+$ complex. The results are shown for delay times of 1 ms (×), 10 ms (□), 100 ms (○), and 1 s (■).

fragment ions was used to understand the factors that affect the competition between different dissociation channels of the complexes.

The energetics and dynamics of proton and electron transfer (PT amd ET) in the dissociation of Co(III)−salen−peptide complexes was examined using a simplified two-channel modeling scheme, in which fragments formed by pathways associated with ET (reactions 1−3, Scheme 1) were summed together and modeled using one rate constant, while the formation of the $[M + H]^+$ ion via reaction 4 was modeled using a different rate constant. Dissociation parameters obtained from the best fit of the experimental data are shown in Table 2. It should be noted that because the PT channel accounts for less than 5% fragmentation of the precursor ion, dissociation parameters obtained for the ET channel largely reflect the relative stability of the complexes toward dissociation.

Table 2. Dissociation Parameters for Proton Transfer (PT) and Electron Transfer (ET) Reactions in Unimolecular Dissociation of Co^{III}(salen)−Peptide Complexes Obtained from the RRKM Modeling

	RVYIHPF		DRVYIHPF		RVYIHDF	
peptide	ET	PT	ET	PT	ET	PT
E_0, eV	1.27	1.35	1.24	1.30	1.24	1.24
$\Delta S^{\ddagger}$, eu[a]	12.9	5.3	13.1	1.5	12.1	1.8
A, s^{-1}	1.7×10^{16}	3.7×10^{14}	1.9×10^{16}	5.3×10^{13}	1×10^{16}	6×10^{13}
log(A)	16.2	14. 6	16.3	13.7	16.9	14.7

[a] eu =entropy unit = cal/(mol K); activation entropies and pre-exponential factors at 450 K. The estimated uncertainties are ±5% for the threshold energies and ±3 eu for the activation entropies.

Modeling results demonstrate that both the dissociation thresholds and the activation entropies associated with the ET pathway are the same within the uncertainty of the model for all cobalt−salen−peptide complexes. This is consistent with the qualitative trends discussed earlier. A similar dissociation threshold was obtained for the PT channel of the $[Co^{III}$(salen)-RVYIHDF$]^+$ complex, while somewhat higher PT threshold energies were obtained for the complexes of RVYIHPF and DRVYIHPF. In contrast, activation entropies of the ET and PT pathways are significantly different. The pre-exponential factors derived from the values of $\Delta S^{\ddagger}$ are 2−3 orders of magnitude lower for the PT reaction. These results suggest that the lower activation entropy of the PT pathway is responsible for the low yield of the $[M + H]^+$ product in the dissociation of all three complexes.

Detailed modeling of the primary dissociation pathways of Co^{III}(salen), Fe^{III}(salen), and Mn^{III}(salen) complexes of RVYIHPF was performed by combining secondary fragments with the corresponding primary fragment ions. The best fit to the experimental data for the $[Co^{III}$(salen)RVYIHPF$]^+$ complex is shown in Figure 11. Clearly, the model provides an excellent fit for the decomposition of the precursor ion and reproduces reasonably well the competition between the primary dissociation channels. The largest uncertainty in the modeling originates from the simplifying assumptions made in attributing secondary fragments to their precursor ions. For example, the $\mathbf{a_5}$ fragment of the $[Co^{III}$(salen)RVYIHPF$]^+$ complex could be produced both from the $M^{+\bullet}$ and from the $M^{+\bullet}-CO_2$ fragment ions. However, the kinetic behavior observed for this fragment suggests that it is mainly produced from the $M^{+\bullet}$ ion.

Dissociation parameters obtained for primary reaction pathways of different complexes are summarized in Table 3. The sensitivity of the modeling parameters to the simplifying assumptions was thoroughly tested and included in the estimated uncertainties. Similar threshold energies and activation entropies were obtained for reactions 2 and 3 (Scheme 1) of the $[Co^{III}$-(salen)RVYIHPF$]^+$ complex, while reactions 1 and 4 are associated with a higher threshold energy and are kinetically more favored. The largest pre-exponential factor of 6×10^{17} s^{-1} was observed for the formation of the radical cation suggesting that this reaction proceeds via a loose transition state (TS) while other three reaction channels are associated with somewhat more tight TS structures. In contrast, the same reaction for the iron−salen complex is associated with a tight TS with a characteristic pre-exponential factor of 8×10^8 s^{-1}. Other primary dissociation channels of this complex and of the $[Mn^{III}$(salen)RVYIHPF$]^+$ complex are characterized by substantially higher threshold energies of 2.45−2.97 eV and very large values of $\Delta S^{\ddagger}$. Surprisingly, the pre-exponential factor for the PT channel of the $[Mn^{III}$(salen)RVYIHPF$]^+$ complex is almost 10 orders of magnitude higher than the corresponding pre-exponential factor obtained for the $[Co^{III}$(salen)RVYIHPF$]^+$ complex. Dissociation of all metal−salen complexes via reaction 5 is a kinetically favorable process characterized by high threshold energy.

3.4. Computational Results. DFT calculations were performed to determine ionization energies of the peptide and the Co^{II}(salen) complex. In these calculations angiotensin III was represented by the RVY tripeptide, in which the C-terminal hydroxyl group was replaced with a methyl group (RVY-Me).

3.4.1. Cobalt−Salen Complex. The Co^{2+} and Co^{3+} ions have the [Ar] $3d^7$ and [Ar] $3d^6$ electron configurations, respectively. As a result, Co^{II}(salen) can exist either as a low-spin ($S = {}^1/_2$) or as high-spin ($S = {}^3/_2$) complex, while Co^{III}(salen)$^+$ has three different spin states ($S = 0, 1, 2$). Calculated relative energies of the Co^{II}(salen) and Co^{III}(salen)$^+$ are summarized in Table 4. According to our calculations the low-spin state of the Co^{II}(salen) ($S = {}^1/_2$) is slightly more stable than the high-spin state ($S = {}^3/_2$) by 1.5 kcal/mol. This result is consistent with the literature data showing that quartet states of Co^{2+} Schiff base complexes lie very close in energy to the doublet states.[41] In contrast, the lowest-energy structure of the Co^{III}(salen)$^+$ complex corresponds to the intermediate ($S = 1$) state that is more stable than the low-spin ($S = 0$) and high-spin ($S = 2$) states by 16.5 and 8.2 kcal/mol, respectively.

Calculated adiabatic and vertical ionization energies (AIE and VIE) of the complex are listed in Table 5. The values show a strong dependence on the initial spin state of the Co^{II}(salen) complex. The AIE and VIE for the $2 \rightarrow 1$ transition are 7.27 and 7.41 eV, respectively, while the corresponding values obtained for the $4 \rightarrow 3$ transition are 6.49 and 7.04 eV, respectively. Comparison with the IE of the Co^{II}(salen) of 7.52 eV reported in the literature[42] suggests that this value most likely corresponds to the ionization of the low-spin state of the neutral complex.

3.4.2. RVY-Me Model Tripeptide. The values of AIE and VIE of 6.04 and 7.36 eV, respectively, were obtained from the most stable structure of the RVY-Me model peptide (Table 5). The AIE of phenol of 8.28 eV obtained at the same level of theory is in good agreement with the previously reported computational value of 8.35 eV[43] and somewhat lower than the experimental AIE value of 8.49 eV.[44] It is likely that other ionization energies listed in Table 5 are underestimated by about 0.2−0.3 eV.

4. Discussion

Our results demonstrate that both the dissociation pathways and the relative stabilities of ternary metal−salen−angiotensin complexes toward fragmentation are strongly affected by the properties of the metal−salen complex and are rather insensitive to the small variations in the primary structure of the peptide as long as the tyrosine residue remains in the sequence.

(41) Kennedy, B. J.; Fallon, G. D.; Gatehouse, B. M. K. C.; Murray, K. S. *Inorg. Chem.* **1984**, *23*, 580−588.
(42) Gilbert, W. C.; Taylor, L. T.; Dillard, J. G. *J. Am. Chem. Soc.* **1973**, *95*, 2477−2482.
(43) Le, H. T.; Flammang, R.; Gerbaux, P.; Bouchoux, G.; Nguyen, M. T. *J. Phys. Chem. A* **2001**, *105*, 11582−11592.
(44) NIST webbook. http://webbook.nist.gov/chemistry.

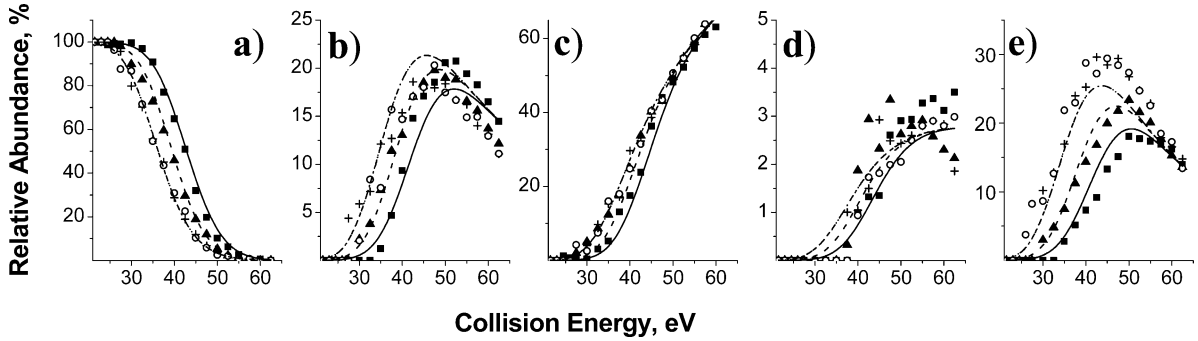

Figure 11. RRKM modeling of the experimental data for dissociation of the $[Co^{III}(salen)RVYIHPF]^+$ complex. Experimental (symbols) and calculated (lines) TFECs for (a) the precursor ion; (b) $[M-COOH]^+$; (c) $M^{+\bullet}$; (d) $[M+H]^+$; and (e) $M^{+\bullet}-CO_2$ ion for reaction delays of 1 ms (■, solid lines), 10 ms (▲, dashed lines), 100 ms (+, dash–dot lines), and 1 s (○, dash–dot–dot lines).

Table 3. Dissociation Parameters for the Primary Reaction Channels of Metal^{III}(salen)–RVYIHPF Complexes Obtained from the RRKM Modeling

fragment	E_0, eV	$\Delta S^{\ddagger}$,[a] eu	A, s^{-1}
	Co^{III}(salen)RVYIHPF		
$M^{+\bullet}$	1.40	20.1	6×10^{17}
$M^{+\bullet}-CO_2$	1.23	4.7	3×10^{14}
$[M-COOH]^+$	1.27	7.3	1×10^{15}
$[M+H]^+$	1.43	11.5	8×10^{15}
$Co^{III}(salen)^+$	2.50	68.0	1×10^{28}
	Fe^{III}(salen)RVYIHPF		
$M^{+\cdot}$	1.23	−20.6	8×10^{8}
$\mathbf{a}_5$	2.45	44.4	1×10^{23}
other a-ions	2.78	60.2	4×10^{26}
$Fe^{III}(salen)^+$	2.97	69.0	3×10^{28}
	Mn^{III}(salen)RVYIHPF		
$Mn^{III}(salen)^+$	2.69	71.2	1×10^{29}
$[M+H]^+$	2.48	55	3×10^{25}

[a] eu = entropy unit = cal/(mol K); activation entropies and pre-exponential factors at 450 K. The estimated uncertainties are ±7% for the threshold energies and ±15% for the activation entropies.

Table 4. Relative Energies of Cobalt-salen Complexes (kcal/mol)[a]

	spin				
species	0	1/2	1	3/2	2
Co^{II}(salen)	–	0.0	–	1.5	–
$Co^{III}(salen)^+$	16.5	–	0.0	–	8.2

[a] Energies obtained from B3LYP/6-31++G(d,p)//B3LYP/6-31G(d) calculations including the ZPE correction. B3LYP/6-31++G(d,p) level of theory was used for C, N, O, and H atoms, and Stuttgart RSC 1997 ECP was used for Co atom.

Table 5. Ionization Energies (IEs) of the RVY-Me and Co^{II}(salen) Complex (eV)[a]

species	spin mulplicity transition	adiabatic IE	vertical IE
Co^{II}(salen)	2 → 1	7.27	7.41
Co^{II}(salen)	4 → 3	6.49	7.04
RVY–Me	1 → 2	6.04	7.36

[a] Energies obtained from B3LYP/6-31++G(d,p)//B3LYP/6-31G(d) calculations including the ZPE correction. B3LYP/6-31++G(d,p) level of theory was used for C, N, O, and H atoms, and Stuttgart RSC 1997 ECP was used for Co atom.

4.1. Cobalt–Salen–Peptide Complexes. For the series of peptide ligands used in this work, dissociation of cobalt–salen–peptide complexes is dominated by the pathways that involve ET from the peptide to the cobalt–salen complex (reactions 1–3, Scheme 1). Replacing tyrosine with glycine results in significant suppression of the formation of the radical cation via reaction 1, while product ions of reactions 2–4 are largely unaffected by such a modification (Figure 4). It follows that the formation of the radical cation from the complex can be mainly attributed to the ET from the tyrosine residue that is axially coordinated to the metal center. This conclusion is in agreement with the observation of very similar energetics and dynamics of the ET channel in the dissociation of cobalt–salen complexes with different angiotensin analogues (Table 2) containing the tyrosine residue.

In contrast, the formation of the $M^{+\bullet}-CO_2$ and $[M-COOH]^+$ fragments from these complexes does not require the presence of the tyrosine residue. Formation of abundant $M^{+\bullet}-CO_2$ and $[M-COOH]^+$ product ions from cobalt–salen–peptide complexes has been also reported by O'Hair and co-workers.[23] The formation of the $M^{+\bullet}-CO_2$ ion is frequently observed in the dissociation of peptides bound to transition metals. It has been suggested that this pathway occurs when the peptide is bound to the metal through the deprotonated C-terminus.[39,45] The ET from the peptide to the metal complex generates a carboxyl radical at the C-terminus (Scheme 2, pathway I). Because carboxyl radicals are fairly unstable in the gas phase,[46] they rapidly decay via the loss of CO_2 to form the $M^{+\bullet}-CO_2$ fragment ion. Alternatively, the carboxyl radical can abstract a hydrogen atom from the methylene group of the side chain of the C-terminal residue (Scheme 2). Because bond dissociation energy of the carboxyl hydrogen (~112 kcal/mol)[47] is greater than the bond dissociation energy of the methylene hydrogen (~98 kcal/mol),[48] such a hydrogen abstraction is exothermic by ca. 14 kcal/mol. If hydrogen abstraction is kinetically favored, the energy released in this step could promote the subsequent $C-C_\alpha$ bond cleavage resulting in efficient loss of the $COOH^\bullet$ group. The proposed mechanism implies that the $COOH^\bullet$ loss is associated with the presence of an acidic hydrogen atom in the side chain of the C-terminal peptide residue. The involvement of the side chain of the C-terminal amino acid in the formation of the $[M-COOH]^+$ fragment ion is confirmed by the fragmentation of the $[Co^{III}(salen)RGGGGYG]^+$ complex (Figure 4c) and $[Co^{III}(salen)RGGGGGG]^+$ complex (not shown), which cannot follow such a mechanism and for which the $[M-COOH]^+$ fragment is not observed. Efficient competition between the CO_2 loss and the $COOH^\bullet$ loss and the striking

(45) Seymour, J. L.; Turecek, F. *J. Mass Spectrom.* **2002**, *37*, 533–540.
(46) Schroder, D.; Soldi-Lose, H.; Schwarz, H. *Aust. J. Chem.* **2003**, *56*, 443–451.
(47) Blanksby, S. J.; Ellison, G. B. *Acc. Chem. Res.* **2003**, *36*, 255–263.
(48) Luo, Y. -R.; Kerr, J. A. Bond Dissociation Energies. *Handbook of Chemistry and Physics*, 87th online ed. http://www.hbcpnetbase.com/.

Scheme 2

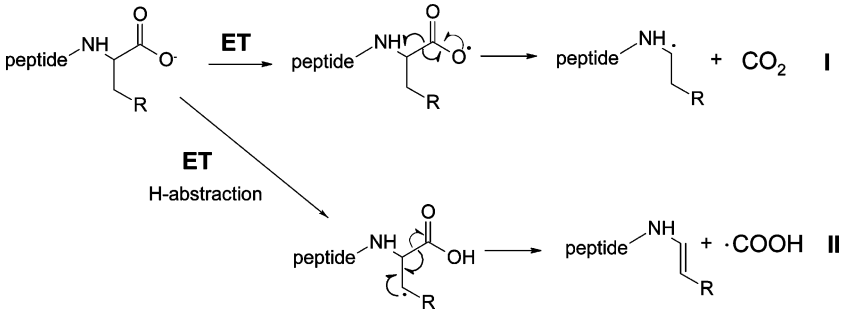

Scheme 3

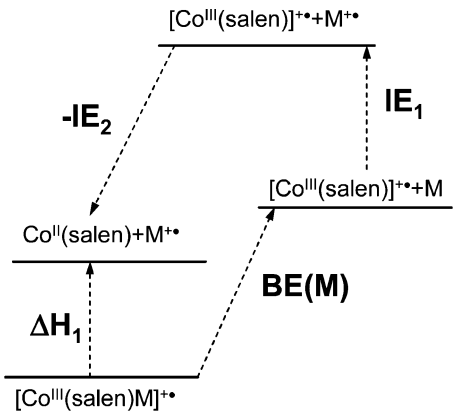

similarity between the dissociation parameters for these two pathways obtained from the RRKM modeling (Table 3) suggest that most likely both fragments are produced from a common precursor as shown in Scheme 2.

Modeling of the competition between the ET and PT pathways in the dissociation of cobalt−salen−peptide complexes (Table 2) demonstrates that low yields of the PT pathway observed in our experiments mainly result from lower activation entropies associated with this reaction channel. Indeed, the energetics of both pathways determined from the modeling is quite similar while the pre-exponential factors obtained for reaction 4 are ca. 2 orders of magnitude lower than the pre-exponential factors for the ET pathway suggesting that for cobalt−salen−peptide complexes reaction 1 is kinetically more favorable. Because both channels are associated with fairly loose transition states, the conformational flexibility of the products may have a pronounced effect on the reaction entropy. It is reasonable to assume that the protonated ion formed by reaction 4 is conformationally more constrained by hydrogen bonding than the radical cation formed by the ET to the complex.

4.2. Thermochemistry of the ET Pathway. Dissociation parameters obtained for different decomposition pathways of the $[Co^{III}(salen)RVYIHPF]^+$ complex can be used to estimate the thermochemical factors that determine the competition between these pathways. The enthalpy of reaction 1 can be expressed in terms of the binding energy of the peptide to the $[Co^{III}(salen)]^+$ ion, BE(M), and the ionization energies (IEs) of the peptide, IE_1, and $Co^{II}(salen)$, IE_2, using the thermochemical cycle shown in Scheme 3. Because reaction 1 proceeds via a loose TS the enthalpy of this reaction can be approximated by the threshold energy shown in Table 3 (i.e., $\Delta H_1 = 1.4$ eV). The binding energy of the neutral peptide to the $[Co^{III}(salen)]^+$ complex estimated from the modeling is BE(M) = 2.5 eV. The difference between the IEs of the $Co^{II}(salen)$ complex, IE_2, and the peptide, IE_1, is given by eq 5:

$$\Delta H_1 = \mathrm{BE(M)} + \mathrm{IE}_1 - \mathrm{IE}_2 \Rightarrow \mathrm{IE}_2 - \mathrm{IE}_1 = \mathrm{E(M)} - \Delta H \approx 2.5\ \mathrm{eV} - 1.4\ \mathrm{eV} = 1.1\ \mathrm{eV} \quad (5)$$

Based on the results reported in this study we estimate that the IE of the complex is ca. 1.1 eV higher than the IE of the peptide. This result is in semiquantitative agreement with the difference between calculated AIEs of the most stable structures of the $Co^{II}(salen)$ ($IE_2 = 7.27$ eV) and the RVY-Me model peptide ($IE_1 = 6.04$ eV) shown in Table 5. The thermochemical analysis presented above suggests that if the IE of the peptide is larger than the IE of the complex, the ET becomes energetically unfavorable.

It is interesting to compare the calculated IEs of the model tripeptide, RVY-Me, with the values reported in the literature for other tyrosine-containing peptides. Dehareng and Dive determined IEs of different conformations of tyrosine-containing tetrapeptides using the outer valence Green's function method.[49] The VIEs of the $\pi 1$(Y) state of the lowest-energy conformations for the family of peptides studied in that work is in the range 7.69−7.80 eV, while the AIEs are in the range 6.17−6.33 eV. Clearly, the IEs of the RVY-Me peptide obtained in our work (VIE = 7.36 eV; AIE = 6.04 eV) are ca. 0.3 eV lower than the values reported by Dehareng and Dive for tetrapeptides containing tyrosine and aliphatic amino acid residues. However, as discussed earlier the values of IEs shown in Table 5 are most likely underestimated by the DFT calculations by 0.2−0.3 eV.

The acidity of the $[Co^{III}(salen)]^+$ can be estimated using a similar thermochemical cycle resulting in eq 6:

$$\Delta H_4 = \mathrm{BE(M)} + \Delta H_{\mathrm{deprot}}(Co^{III}(salen)^+) - \mathrm{PA(M)} \Rightarrow \Delta H_{\mathrm{deprot}}(Co^{III}(salen)^+) - \mathrm{PA(M)} = \Delta H_4 - \mathrm{BE(M)} \approx 1.43\ \mathrm{eV} - 2.5\ \mathrm{eV} \quad (6)$$

It follows from eq 2 that the proton affinity (PA) of the peptide is larger than the deprotonation enthalpy of the complex by ca. 1.1 eV. In contrast, the difference between the PA of the peptide and the deprotonation enthalpy of the $[Mn^{III}(salen)]^+$ complex is only 0.2 eV suggesting that the acidity of the metal−salen complex strongly depends on the properties of the metal.

Peptide Complexes with $Fe^{III}(salen)^+$ and $Mn^{III}(salen)^+$. Fragmentation of $Fe^{III}(salen)^+$ and $Mn^{III}(salen)^+$ complexes with angiotensin III is very different from the dissociation behavior of $Co^{III}(salen)^+$ complexes discussed earlier. Specifically, products of reactions 2 and 3 are not observed for these

(49) Dehareng, D.; Dive, G. *J. Phys. Chem. A* **2006**, *110*, 11975−11987.

complexes, while dissociation of the complex into the Metal^{III}(salen)$^+$ ion and the neutral peptide molecule (reaction 5) is a dominant channel. The formation of the peptide radical cation via reaction 1 is a major fragmentation pathway for the iron−salen complex and is not observed for the manganese−salen complex; the PT channel is observed for both complexes. In addition, ternary complexes of these metals are significantly more stable toward dissociation than the cobalt−salen−peptide complex. Most of our findings are consistent with the results reported by O'Hair and co-workers for dissociation of metal−salen complexes with YGGFLR as a peptide ligand.[23] For example, in their study $M^{+\bullet}-CO_2$ and $[M-COOH]^+$ fragments were observed only for the $[Co^{III}(salen)YGGFLR]^+$ complex. They also observed abundant loss of the neutral peptide from the manganese−salen complex. However, for this peptide ligand formation of the $M^{+\bullet}$ fragment ion is a dominant channel for all three metal complexes, while in our study we observed strong suppression of this reaction for the manganese−salen complex.

The formation of the radical cation is the lowest-energy pathway in the dissociation of the [iron-salen]$^+$ complex. The threshold energy for this channel (1.23 eV) is somewhat lower than the threshold energy for the same pathway of the [cobalt-salen]$^+$ complex. However, dissociation of the Fe^{III}(salen)$^+$ complex via reaction 1 proceeds via a tight transition state and hence is kinetically hindered. The activation entropy obtained for this reaction from the modeling is ca. 40 eu lower and the pre-exponential factor is almost 9 orders of magnitude lower than the activation entropy and the pre-exponential factor of reaction 1 obtained for the [cobalt-salen]$^+$ complex. Kinetically hindered formation of the peptide radical cation from the iron−salen−peptide complex is also reflected in the shapes of TFECs for the $M^{+\bullet}$ product ion of the two complexes shown in Figure 10. In spite of the lower dissociation threshold, the experimental onset for the peptide radical cation formation from the iron−salen complex is shifted by more than 25 eV toward higher collision energies as compared to the onset obtained for this reaction from the cobalt−salen complex suggesting that dissociation of the iron−salen complex is characterized by a substantially larger kinetic shift.[50,51] In addition, the $M^{+\bullet}$ fragment of the iron−salen complex is completely suppressed at short reaction delays and becomes dominant only for delay times longer than 10 ms, while this fragment ion is readily formed from the cobalt−salen complex at all delay times examined in our SID experiments.

The differences in dissociation of the iron−salen and cobalt−salen complexes most likely indicate the different mode of binding of the peptide in these complexes. MS/MS results shown in Figure 4 suggest that reaction 1 is promoted by the presence of the tyrosine residue in the peptide sequence. Fast formation of the radical cation from the cobalt−salen complex indicates that the tyrosine residue is involved in the binding between the peptide and the $[Co^{III}(salen)]^+$ complex. In contrast, negative activation entropy associated with this reaction from the iron−salen complex suggests that the tyrosine residue is remote from the metal complex and substantial rearrangement is required to bring this residue close to the metal center. Suppression of the $M^{+\bullet}-CO_2$ and $[M-COOH]^+$ product ions for the iron−salen complex could indicate that the C-terminal carboxyl group of the peptide is also not involved in the binding to the metal or that the ET from the carboxyl group to the $[Fe^{III}(salen)]^+$ complex is a thermochemically unfavorable process.

The structures and redox properties of metal−salen complexes in solution have been extensively investigated.[52−54] Mn^{III}(salen) and Fe^{III}(salen) are high-spin complexes[52,55] while Co^{III}(salen) is most likely a low-spin complex similarly to other complexes of Co(III).[56] However, Beauchamp and co-workers showed that in the gas phase the Co^{III}(salen) complex exists in the high-spin or intermediate-spin state.[57] The reduction potentials are −0.45 V for Mn^{III}(salen),[54] −0.28 V for Fe^{III}(salen),[54] and −0.26 V for Co^{III}(salen)[58] referenced to the SCE electrode. The reported trend in reduction potentials suggests that Co^{III}(salen)$^+$ and Fe^{III}(salen)$^+$ complexes are better oxidizing agents than the manganese−salen complex. Peptide coordination may affect the redox potentials, but the trend is expected to be the same. This suggests that the electron affinity in the gas phase follows the order Co ≈ Fe > Mn. Suppression of the ET pathways for the $[Mn^{III}(salen)RVYIHPF]^+$ complex observed in this study is in agreement with this assertion.

The formation of the $\mathbf{a_5}$ ion corresponding to the cleavage between histidine and proline is a preferred primary pathway in the dissociation of the $[Fe^{III}(salen)RVYIHPF]^+$ complex.[59] Histidyl residues play an important role in metal chelation in a variety of metalloproteins.[60−62] Previous studies showed that selective fragmentation C-terminal to the histidine residue is common for peptides cationized on transition metals.[40,63] In addition, enhanced cleavage N-terminal to the proline residue has been reported for a variety of protonated peptide ions.[64,65] It follows that the formation of the abundant $\mathbf{a_5}$ ion could be attributed to the presence of the histidine and the proline residues in the peptide sequence. In order to test this suggestion we conducted SID experiments for iron−salen complexes of RVYIFPF and RVYIHAF and compared them with the results obtained for RVYIHPF. Very similar SID spectra (not shown) were obtained for all three peptide ligands suggesting that the presence of the histidine and the proline residues does not have a significant effect on the formation of the $\mathbf{a_5}$ ion. It should be noted that the formation of the abundant $\mathbf{a_{n-2}}$ ion is a common pathway in fragmentation of radical cations of angiotensin

(50) Lifshitz, C. *Eur. J. Mass Spectrom.* **2002**, *8*, 85−98.
(51) Laskin, J. Energy and Entropy Effects in Gas-Phase Dissociation of Peptides and Proteins. In *Principles of Mass Spectrometry Applied to Biomolecules*; Laskin, J., Lifshitz, C., Eds.; John Wiley & Sons: Hoboken, NJ, 2006
(52) Hobday, M. D.; Smith, T. D. *Coord. Chem. Rev.* **1972**, *9*, 311−337.
(53) Yamada, S. *Coord. Chem. Rev.* **1999**, *192*, 537−555.
(54) Venkataramanan, N. S.; Kuppuraj, G.; Rajagopal, S. *Coord. Chem. Rev.* **2005**, *249*, 1249−1268.
(55) Barone, G.; Silvestri, A.; La Manna, G. *THEOCHEM* **2005**, *715*, 79−83.
(56) Garcia, Y.; Gutlich, P. *Top. Curr. Chem.* **2004**, *234*, 49−62.
(57) Lee, S. W.; Chang, S. B.; Kossakovski, D.; Cox, H.; Beauchamp, J. L. *J. Am. Chem. Soc.* **1999**, *121*, 10152−10156.
(58) Huber, A.; Muller, L.; Elias, H.; Klement, R.; Valko, M. *Eur. J. Inorg. Chem.* **2005**, 1459−1467.
(59) Although this fragment is also observed for $[Co^{III}(salen)RVYIHPF]^+$ and $[Mn^{III}(salen)RVYIHPF]^+$ precursors, collision energy dependent data shown in Figures 2, 6, and 7 suggest that, for the $[Co^{III}(salen)RVYIHPF]^+$ complex, the $\mathbf{a_5}$ ion is formed by consecutive fragmentation of the $M^{+\bullet}$ ion, while, for $[Mn^{III}(salen)RVYIHPF]^+$, this fragment is produced directly from the precursor ion but at much higher collision energies and with much lower relative abundance than the case for $[Fe^{III}(salen)RVYIHPF]^+$.
(60) Sundberg, R. J.; Martin, R. B. *Chem. Rev.* **1974**, *74*, 471−517.
(61) Lombardi, A.; Nastri, F.; Pavone, V. *Chem. Rev.* **2001**, *101*, 3165−3190.
(62) Wu, A. J.; Penner-Hahn, J. E.; Pecoraro, V. L. *Chem. Rev.* **2004**, *104*, 903−938.
(63) Loo, J. A.; Hu, P. F.; Smith, R. D. *J. Am. Soc. Mass Spectrom.* **1994**, 5, 959−965.
(64) Tang, X. J.; Thibault, P.; Boyd, R. K. *Anal. Chem.* **1993**, *65*, 2824−2834.
(65) Vaisar, T.; Urban, J. *J. Mass Spectrom.* **1996**, *31*, 1185−1187.

analogues.[14,66] It follows that the formation of this fragment does not necessarily require the presence of the metal complex. Competition between the formation of the $\mathbf{a_5}$ ion and the $M^{+\bullet}$ ion from the $[Fe^{III}(salen)RVYIHPF]^+$ complex could be responsible for rather inefficient formation of the radical cation as compared to the results reported by O'Hair and co-workers for complexes of iron-salen with a different class of ligands.[23]

Finally, we note that most of the dissociation pathways of the iron−salen and the manganese−salen complexes are characterized by very large activation entropies and high threshold energies. The large activation entropies are most likely associated with the change in the conformational entropy between the free peptide and the peptide coordinated to the metal complex. It is remarkable that the pre-exponential factors obtained for the kinetically hindered electron-transfer reaction (reaction 1) and the loss of the neutral peptide (reaction 5) from the $[Fe^{III}(salen)RVYIHPF]^+$ complex differ by almost 20 orders of magnitude and the dissociation thresholds differ by ca. 1.7 eV. To the best of our knowledge this is the first observation of the competition between gas-phase fragmentation reactions with such dramatic differences in the kinetic behavior.

5. Conclusions

We report here the first detailed study of the factors that affect gas-phase fragmentation of ternary complexes of angiotensin analogues with trivalent metal−salen systems. Time- and collision-energy-resolved SID provide interesting insight on the competition between proton transfer, electron transfer, and loss of the neutral peptide ligand in these model systems. We found that both the fragmentation behavior and the stability of the complexes are similar for different peptide ligands examined in this study. In contrast, the observed fragmentation pathways, the mode of binding, and the energetics and dynamics of dissociation of these systems strongly depend on the electronic properties of the metal center. RRKM modeling of the experimental data revealed that the competition between the proton transfer and electron transfer in the dissociation of cobalt−salen complexes is mainly determined by the differences in entropy effects while the energetics of both pathways are quite similar. Formation of $M^{+\bullet}-CO_2$ and $[M-COOH]^+$ fragments from cobalt−salen−peptide complexes was attributed to the electron transfer from the C-terminal carboxyl group coordinated to the cobalt−salen core, while the $M^{+\bullet}$ fragment is mainly formed by the electron transfer from the tyrosine residue that is axially coordinated to the metal center. The electron transfer to the C-terminal carboxyl group was not observed for the $[Fe^{III}(salen)RVYIHPF]^+$ complex suggesting that this group most likely is not involved in metal chelation. Interestingly, a very different kinetics of formation of the $M^{+\bullet}$ fragment ion from the cobalt−salen and iron−salen complexes was observed experimentally. We concluded that the electron-transfer process in the dissociation of the $[Fe^{III}(salen)RVYIHPF]^+$ ion requires substantial rearrangement of the complex. As a result, the formation of the radical cation from the iron−salen complex requires a much higher collision energy as compared to the cobalt−salen complex. Complete suppression of the electron-transfer pathway in the dissociation of the $[Mn^{III}(salen)RVYIHPF]^+$ ion is attributed to the low electron affinity of the $Mn^{III}(salen)^+$ complex. Our results are in good qualitative agreement with the redox properties of these complexes reported in the literature.

Acknowledgment. This study was partially supported by the grant from the Chemical Sciences Division, Office of Basic Energy Sciences of the U.S. Department of Energy and partially by the University of Hong Kong and Hong Kong Research Grant Council, Special Administrative Region, China (Project No. 7019/05P). The authors would like to thank Dr. Corey Lam for providing metal−salen complexes and Dominic C. M. Ng and Minjie Xu for technical assistance with some experiments and for helpful discussions. The authors also thank Drs. Jun Li and Niri Govind for helpful suggestions regarding the electronic structure calculations. Most of the research described in this manuscript was performed at the W. R. Wiley Environmental Molecular Sciences Laboratory (EMSL), a national scientific user facility sponsored by the U.S. Department of Energy's Office of Biological and Environmental Research and located at Pacific Northwest National Laboratory (PNNL). PNNL is operated by Battelle for the U.S. Department of Energy. I.K.C. acknowledges participation in the PNNL Interfacial and Condensed Phase Summer Research Institute.

Supporting Information Available: Complete ref 30 and 32. This material is available free of charge via the Internet at http://pubs.acs.org.

JA077690S

(66) Chu, I. K.; Lam, C. N. W. *J. Am. Soc. Mass Spectrom.* **2005**, *16*, 1795−1804.